Optics Letters

High-repetition-rate pulse generation via self-sustaining cross-gain modulation in a semiconductor-based laser

Sergey Smirnov,[1,*] Boris Nyushkov,[1,2] Aleksey Ivanenko,[1] and Anastasia Bednyakova[1]

[1]Novosibirsk State University, Novosibirsk, 630090, Russia
[2]Novosibirsk State Technical University, Novosibirsk, 630073, Russia
*sergeyv.smirnov@gmail.com

Received 29 September 2023; revised 26 October 2023; accepted 27 October 2023; posted 30 October 2023; published 15 November 2023

We present a simple and efficient method for generating regular pulse trains with GHz pulse repetition rates in lasers based on semiconductor optical amplifiers (SOAs). This method enables pulse formation without active modulation or saturable absorption of the generated radiation. The method relies upon the self-sustaining cross-gain modulation which is achieved by adding the negative optical feedback (NOF) to a ring laser configuration. The resulting modulation of laser gain is shown to be restricted to the frequencies which match both the spacing of longitudinal laser modes and the highest peaks in the NOF-induced instability gain spectrum. This enables the reproducible stationary pulse generation at the strictly defined repetition rates. The feasibility of the method was confirmed by the stable generation of sub-nanosecond pulses at repetition rates up to 1.79 GHz in a SOA-based laser with a simple fiber cavity.

https://doi.org/10.1364/OL.506902

Novel and effective physical mechanisms for generating short and ultra-short pulses in lasers are of interest for both fundamental physics and laser technologies [1]. This stimulates invention of the completely new methods for pulse generation (e.g., via dissipative Faraday instability [2] or transient light shift register mechanism [3]), which unlike primary methods do not rely upon active modulation or saturable absorption of radiation.

In this Letter, we introduce an original method for high-repetition-rate (GHz) pulse generation which relies upon the self-sustaining cross-gain modulation in a semiconductor optical amplifier (SOA)-based laser with the negative optical feedback (NOF). This method features remarkable simplicity in comparison with the active modulation techniques typically employed for pulse generation at GHz repetition rates in SOA-based lasers [4–7]. It also ensures compactness and overall energy efficiency of lasers owing to the all-electrical pumping and the non-dissipative pulse shaping. The method is not associated with the Kerr nonlinearity and does not require particular nonlinear cavity arrangements (like a nonlinear amplifying loop mirror used in [8]). Therefore, it can be potentially implemented by using various (fiber, waveguide, discrete) optics in the laser cavity design.

The cross-gain modulation (XGM) phenomenon underlying the method was previously used for performing operations in all-optical logical schemes [9,10] as well as for the active mode-locking in lasers through the injection of modulating optical pulses from external sources into SOAs [5,11,12]. The resulting SOA gain modulation was determined by the complex characteristics of modulating optical pulses coming from external sources which had to be precisely adjusted to satisfy the active mode-locking conditions in SOA-based lasers [13].

Herein, the NOF added to a ring SOA-based laser induces XGM-related instability. We demonstrate that the resulting self-sustaining modulation of the laser gain is restricted to the frequencies which match both the spacing of longitudinal laser modes (the inter-mode frequency) and the highest peaks in the NOF-induced instability gain spectrum. Such restricted XGM instability can reproducibly trigger stationary self-sustained pulse generation as shown below with a test-bed laser.

In the proposed laser configuration shown in Fig. 1, the NOF re-injects a portion of generated radiation into the SOA in the direction opposite to the unidirectional lasing sustained by the positive optical feedback (POF). Temporal variations of the overall optical power delivered into the SOA by the POF and NOF cause corresponding variations of the SOA gain, owing to its fast saturation and recovery as illustrated by the inset in Fig. 1. At certain frequencies, such gain variations align in phase with variations of the generated wave power (*i. e.* the higher the power, the greater the gain). This makes continuous-wave (CW) generation unstable and leads to formation of a stationary regular pulse train.

To implement the proposed laser configuration, we used a commercial SOA "Rayzer" (see Supplement 1 for specification) and polarization-maintaining fiber-optics elements. The essential elements are the 40/60 coupler and the circulator, which jointly form the POF and NOF loops. The bandpass filter and the 5/95 coupler are optional elements used, respectively, to select the lasing wavelength and to monitor both the POF- and NOF-associated radiation. The length of the POF loop forming the laser cavity was about 743 cm, which corresponds to

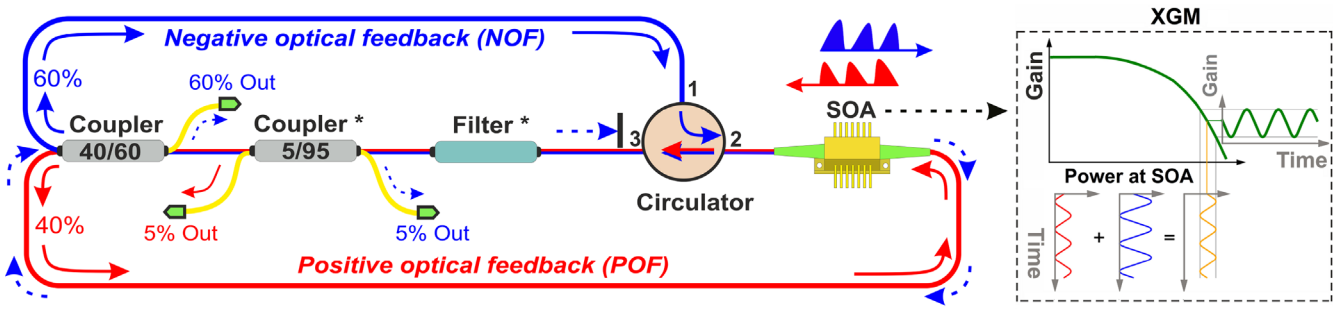

Fig. 1. Laser setup for pulse generation via the self-sustaining XGM. Dashed blue arrows indicate the re-injected NOF-associated radiation which finally gets blocked by the port 3 of the circulator. Asterisks mark elements that are not essential for pulse shaping.

the frequency interval of 27.48 MHz between longitudinal laser modes (the inter-mode frequency). The overall NOF length (including the segment shared with the POF) was about 1020 cm. Stationary pulse generation was self-triggered once the lasing threshold was significantly surpassed with the SOA pump current reaching above 350 mA. The pulse generation started at a repetition rate of 1.567 GHz corresponding to the 57th harmonic of the inter-mode frequency. By further manipulating the laser gain or loss (through the SOA current tuning or intracavity fiber bending), it was possible to reliably switch the laser also to the pulse repetition rates of 1.347 GHz and 1.786 GHz (the 49th and 65th harmonics of the inter-mode frequency, respectively). These frequencies match the strongest peaks in the NOF-induced instability gain spectrum as shown further in the theoretical analysis.

Once triggered, pulse generation at the highest repetition rate of 1.786 GHz remained stable for an unlimited time even upon smooth variation of the SOA current in the range of 250 to 550 mA. Below we report characteristics acquired at 450 mA.

Figure 2 (a) shows lengthy discrete series of time trace pairs which represent both the generated pulse train and its complementary NOF-associated replica passed through the SOA in the opposite direction. The series were collected synchronously at 1 min intervals over the course of 1 h, by means of a real-time oscilloscope and a pair of fast photodiodes coupled to the both output ports of the 5/95 coupler. These observations provide qualitative evidence of the pulse train regularity and stability and also demonstrate mutual timing of the NOF- and POF-associated pulses, accounting for difference in their propagation delays from the SOA to the oscilloscope. The generated pulse train features a relatively large duty cycle close to a half, which is preferable in telecommunications [14]. By measuring radio-frequency (RF) spectra of the generated pulse train, we quantitatively evaluated its noise characteristics and validated that the pulse repetition rate match certain harmonic of the inter-mode frequency. The measured RF spectra are shown in Fig. 2 (b). Despite the presence of weak sidebands (spurious signals with fluctuating amplitudes at offset frequencies of ±1.1 and ±2.2 MHz), the RF spectra feature a relatively high signal-to-noise ratio of about 60 dB, which is comparable to that of mode-locked laser radiation.

The measured optical spectra of the generated pulse trains feature a full width at half maximum of about 0.1 nm [Fig. 2 (c)]. Such narrowband pulse generation is well suited for telecom and metrology applications.

We also measured and compared the average powers delivered by the NOF- and POF-associated pulse trains to the available

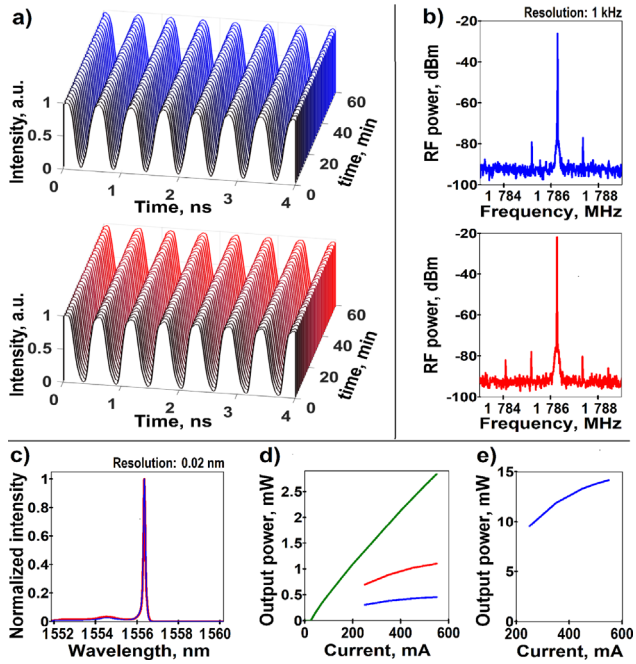

Fig. 2. (a) Synchronously measured series of time traces of the generated NOF- and POF-associated pulse trains. (b) and (c) RF spectra and overlaid optical spectra of the generated pulse trains, respectively. (d) and (e) Dependencies of the average output power at the 5/95 and 40/60 couplers (respectively) on the SOA current. Legend of the plots: the blue and red curves characterize the NOF- and POF-associated pulsed radiation, respectively, while the green curve – the POF-associated CW radiation obtainable upon breaking the NOF loop.

output couplers' ports. Figures 2 (d)–2 (e) represent the measured output powers versus the SOA current. Finally, we broke the NOF loop to reveal its impact. With the open NOF loop, the laser sustained only CW generation. The output power characteristic of such CW generation is represented in Fig. 2 (d) by the green curve. One can see that the NOF noticeably affects the laser power characteristics. The NOF redistributes the laser energy between the two counter-directional flows modulating each other via XGM in the SOA. The NOF-associated pulses experience extra amplification when re-injected into the SOA. Therefore, more powerful pulses can be obtained via the 60% tap of the 40/60 coupler. The average output power at this tap reached 14.2 mW as seen in Fig. 2 (e).

Pulse generation characteristics were well reproduced with repeated turning off and on of the laser, e.g., the pulse repetition rates were reproduced with a kilohertz accuracy.Optional features of pulse generation at the lower repetition rates are shown in Supplement 1.

To gain insight into the underlying physical factors behind the emergence of pulses in the proposed hybrid fiber-semiconductor laser system, we undertake the stability analysis of the CW solution, utilizing the simplest mathematical model, that encompasses the primary physical effects such as SOA saturable gain, lumped losses, and time delay in two fiber feedback loops. Assuming a stable state of CW laser generation, we can express the power $P_+^{(\mathrm{out})}$ of the wave that has passed through the positive feedback loop at the output of the SOA as a weak modulation on a stationary background:

$$P_+^{(\mathrm{out})} = P^{(0)} + P^{(1)} \cos \Omega t, \tag{1}$$

where t stands for time, Ω denotes a modulation frequency, $P^{(0)}$ is the background power level corresponding to the stationary lasing condition, and $P^{(1)} \ll P^{(0)}$ is a small modulation amplitude, which can arise from technical noises in the power supply circuit of the SOA or from weak external influences on the whole laser system. Once the wave (1) travels within the cavity, it is split into two replicas, each of which goes through its own feedback loop, either positive or negative, and eventually reaches the corresponding input of the SOA:

$$P_\pm'^{(\mathrm{in})} = |\alpha_\pm| P^{(0)} + P^{(1)} \Re\{\alpha_\pm e^{-\mathrm{i}\Omega t}\}. \tag{2}$$

Here the prime symbol above P represents the power after completing one round trip within the cavity; $P^{(\mathrm{in})}$ denotes the input power of the SOA; the signs $\pm$ in the subscripts indicate the corresponding feedback loops; α represents the complex transmittance of the loop, with its modulus $|\alpha_\pm|<1$ being equal to the power transmittance coefficient, whereas its argument $\arg\{\alpha_\pm\} = \Omega L_\pm n/c$ determines the phase delay of the wave propagating at speed c/n in a feedback loop of length $L_\pm$; $\mathrm{i}^2 = -1$, and $\Re\{z\}$ is the real part of the complex number z.

For the sake of simplicity, let us assume that the SOA gain can be represented in the form:

$$g = g_0 \cdot \left(1 + \langle P \rangle / P_{\mathrm{sat}}\right)^{-1}, \tag{3}$$

where g_0 and P_{sat} are the SOA small-signal gain and saturation power, respectively, and $\langle P \rangle$ is the total input power of the SOA averaged over a relaxation time of γ^{-1}:

$$\langle P \rangle = \gamma \int_0^{+\infty} P_\Sigma^{(\mathrm{in})}(t - t') e^{-\gamma t'} \, \mathrm{d}t', \tag{4}$$

where $P_\Sigma^{(\mathrm{in})} = P_+^{(\mathrm{in})} + P_-^{(\mathrm{in})}$. Substituting here $P_\pm^{(\mathrm{in})}$ from Eq. (2), we obtain

$$\langle P \rangle = \tilde{\alpha} P^{(0)} + \Re\{\alpha P^{(1)} \zeta e^{-\mathrm{i}\Omega t}\}, \tag{5}$$

where $\alpha = \alpha_+ + \alpha_-$, $\tilde{\alpha} = |\alpha_+| + |\alpha_-|$, and $\zeta = \gamma/(\gamma - \mathrm{i}\Omega)$. With the use of Eqs. (2)–(5), the power $P_+'^{(\mathrm{out})} = g P_+'^{(\mathrm{in})}$ after a whole cavity round trip can be written in a linear approximation with respect to the small ratio $P^{(1)}/P^{(0)}$:

$$P_+'^{(\mathrm{out})} = \frac{|\alpha_+| g_0}{1 + \tilde{\alpha} P^{(0)} P_{\mathrm{sat}}^{-1}} P^{(0)} + \frac{g_0 \Re\{\alpha_+ e^{-\mathrm{i}\Omega t}\}}{1 + \tilde{\alpha} P^{(0)} P_{\mathrm{sat}}^{-1}} P^{(1)} - \frac{g_0 |\alpha_+| P^{(0)} P_{\mathrm{sat}}^{-1} \Re\{\alpha \zeta e^{-\mathrm{i}\Omega t}\}}{(1 + \tilde{\alpha} P^{(0)} P_{\mathrm{sat}}^{-1})^2} P^{(1)}. \tag{6}$$

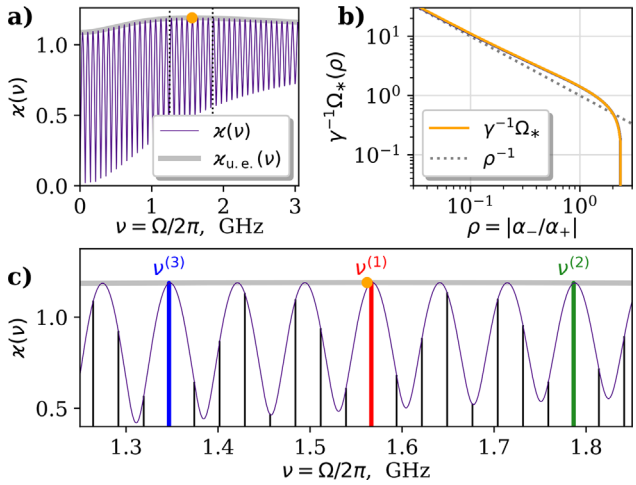

Fig. 3. (a) Dependence of the power modulation growth factor $\varkappa$ and its upper envelope $\varkappa_{\mathrm{u.e.}}$ on the modulation frequency ν for the estimated parameters of the experimental setup. The maximum point of $\varkappa_{\mathrm{u.e.}}(\nu)$ is highlighted in orange. (b) Dependence of the position of the maximum on the curve $\varkappa_{\mathrm{u.e.}}(\nu)$ *versus* $\rho = \alpha_-/\alpha_+$. (c) Enlarged fragment of the graph in panel (a) enclosed in a dotted box; vertical black lines indicate cavity mode intervals; the colored thick lines represent the three frequencies corresponding to the three highest values of $\varkappa$.

In the zeroth order of the expansion with respect to $P^{(1)}/P^{(0)}$, the stationarity condition for laser generation is equivalent to the coefficient at $P^{(0)}$ in the first term of Eq. (6) being equal to unity. By imposing this condition, we can determine the ratio of the power modulation amplitudes at the end and at the beginning of the cavity round trip:

$$\varkappa = \left| 1 - \frac{q}{1 - \mathrm{i}\Omega\gamma^{-1}} \left(1 + \left| \frac{\alpha_-}{\alpha_+} \right| \exp\left(\frac{\mathrm{i}\Omega \delta L}{c/n} \right) \right) \right|. \tag{7}$$

Here, $q = P^{(0)} P_{\mathrm{sat}}^{-1} g_0^{-1} = (|\alpha_+| - g_0^{-1})/(|\alpha_+| + |\alpha_-|) < 1$ and $\delta L = L_- - L_+$ are both real constants. Figure 3 (a) shows the dependence of $\varkappa(\nu)$, where $\nu = \Omega/2\pi$, with parameters close to those used in the experiment. It is evident that the function $\varkappa(\nu)$ oscillates with a period of $(c/n)/|\delta L|$, and the condition for growth of modulation amplitude, $\varkappa > 1$, is simultaneously satisfied across multiple frequencies. It is expected that the gain competition will result in the decay of a continuous wave into pulses with a frequency corresponding to the maximum value of $\varkappa(\nu)$. To determine this maximum, it is useful to examine the upper envelope of the fast oscillations of the function $\varkappa(\nu)$, as depicted by the thick gray line in Fig. 3 (a), which follows the equation:

$$\varkappa_{\mathrm{u.e.}} = 1 + \frac{q^2(1 + \rho^2) - 2q}{1 + (\Omega/\gamma)^2} + 2q\rho \frac{\sqrt{(\Omega/\gamma)^2 + (1 - q)^2}}{1 + (\Omega/\gamma)^2}, \tag{8}$$

where $\rho = |\alpha_-/\alpha_+|$. Since $g_0^{-1} \ll |\alpha_+|$, $q \approx (1 + \rho)^{-1}$, indicating that $\operatorname{argmax}\{\varkappa_{\mathrm{u.e.}}(\Omega/\gamma)\}$ depends solely on ρ. The plot of $\Omega_* = \operatorname{argmax}\{\varkappa_{\mathrm{u.e.}}(\Omega)\}$ is shown as a solid line in Fig. 3 (b), whereas the dotted line on the same graph demonstrates the asymptotic behavior of $\gamma^{-1}\Omega_*(\rho) \sim \rho^{-1}$. For our experimental setup, $\rho = 1.19$, resulting in $\gamma^{-1} \operatorname{argmax}\{\varkappa_{\mathrm{u.e.}}(\Omega)\} = 1.178$. By knowing the preferred pulse repetition rate in the experiment, $\nu = 1567$ MHz, we can estimate $\gamma^{-1} = 1.178/(2\pi\nu) = 120$ ps.

By adjusting the arm lengths $L_\pm$ around the measured experimental values to better align with the three observed pulse

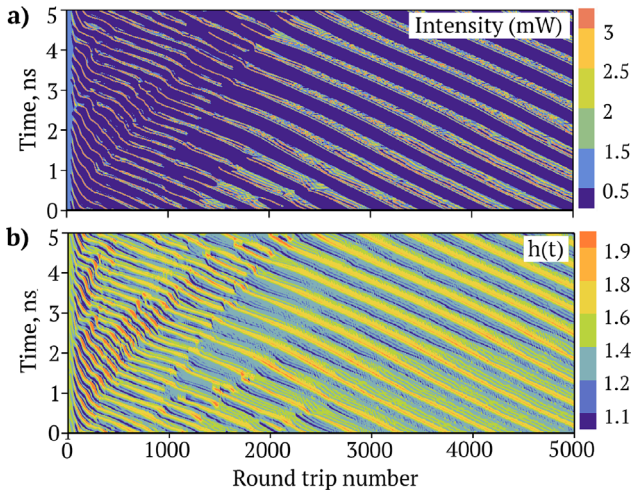

Fig. 4. (a) The build-up dynamics of the output pulse train at a repetition rate of 1.786 GHz calculated using the full model. (b) Modulated SOA gain.

repetition frequencies in the experiment, we obtained $L_+ = 742.55$ cm and $L_- = 1020.08$ cm. Figure 3 (c) corresponds to these determined values and displays an enlarged fragment of the $\varkappa(\nu)$ plot, which is marked by a dotted rectangle in Fig. 3 (a). The vertical lines in Fig. 3 (c) represent the intervals between different cavity modes: $\Omega_m = 2\pi\nu_m = m(c/n)L_+^{-1}$. The three frequencies associated with the three highest values of $\varkappa(\nu_m)$ are depicted as bold colored lines: $\nu^{(1)} = 1566.6$ MHz, $\nu^{(2)} = 1786.5$ MHz, and $\nu^{(3)} = 1346.7$ MHz. Note that the factors $\varkappa$ for these three frequencies are very close, allowing for easy frequency switching through slight adjustments to the system parameters (*e.g.*, modifying the SOA current or introducing minor losses through fiber bending) or depending on the initial noise fluctuations upon laser turning on.

As demonstrated above, even in such a simplistic model, continuous generation becomes unstable against exponentially growing power modulations occurring at sub-GHz and GHz frequencies. However, this model is no longer valid after CW generation breakup, and therefore, to investigate the formation of pulse trains, it is necessary to employ a more accurate model and numerical simulations for integrating the corresponding equations. Numerical modeling of the intra-cavity light dynamics has been implemented by a consecutive computation of optical field evolution represented as $A_\pm = \sqrt{P_\pm} \cdot \exp(i\phi_\pm)$, where $P_\pm$ denotes power and $\phi_\pm$ denotes phase, in the laser elements (see Supplement 1 for details). We employed a more accurate model for the SOA, which includes modification of the intput field $A_+^{(\mathrm{in})}(t)$ by the amplification: $A_+^{(\mathrm{out})}(t) = \exp\left[(1 - i\alpha_H)h(t)/2\right] A_+^{(\mathrm{in})}(t)$, and a differential equation for the time-dependent gain $h(t)$ [15]:

$$\frac{dh}{dt} = -\frac{h - h_0}{T_{SOA}} - \frac{|A_+^{(\mathrm{in})}(t)|^2 + |A_-^{(\mathrm{in})}(t)|^2}{E_{sat}} \left[\exp(h) - 1\right], \qquad (9)$$

where $\alpha_H = 4$ is the linewidth enhancement factor, $h_0 = 18$ dB is the integral small-signal gain, $T_{SOA} = 400$ ps is the gain recovery time, $E_{sat} = 6$ pJ is a characteristic saturation energy. The equation was solved using the second-order Runge–Kutta method. At the onset of the first cavity round trip, the field amplitude was initialized as a constant CW wave with additive "white" Gaussian noise at a level of -30 dB. The simulations are run for $\sim 10^5$ cavity round trips until the field reaches the steady state. The output field and SOA gain evolution versus the round-trip number are shown in Figs. 4(a) and 4(b), respectively. Breakup of the CW radiation into a train of short pulses occurs at the 3 GHz, and after the first 3000–4000 cavity round trips, the repetition rate converges down to 1.786 GHz. Note that changing the seed of the initial random noise in simulations led to pulse train generation at particular repetition rates (either 1.347, 1.567, or 1.786 GHz). Thus, the results of numerical simulations demonstrate that NOF-induced instability yields to the generation of the regular pulse trains and agree well both with stability analysis and experimental observations.

In conclusion, it was shown that introducing NOF into a SOA-based laser is a simple, reliable, and efficient method for achieving high-repetition-rate pulse generation. The underlying physical mechanism is the self-sustaining XGM which was explored as a novel, intrinsic driver for stationary pulse operation of SOA-based lasers. We anticipate this mechanism to be ultimately as fast as the SOA gain recovery, potentially enabling a correspondingly high pulse repetition rate (up to 5 GHz in typical SOAs, assuming a gain recovery time of about 0.2 ns).

Funding. Russian Science Foundation (21-42-04401).

Acknowledgment. We are grateful to Prof. Sergei Turitsyn for intellectual inspiration and to Dr. Ilya Vatnik for technical support.

Disclosures. The authors declare no conflicts of interest.

Data availability. Data underlying the results presented in this paper are not publicly available at this time but may be obtained from the authors upon reasonable request.

Supplemental document. See Supplement 1 for supporting content.

REFERENCES

1. W. Fu, L. G. Wright, P. Sidorenko, *et al.*, Opt. Express **26**, 9432 (2018).
2. N. Tarasov, A. M. Perego, D. V. Churkin, *et al.*, Nat. Commun. **7**, 12441 (2016).
3. B. Nyushkov, A. Ivanenko, S. Smirnov, *et al.*, Optica **10**, 1029 (2023).
4. N. V. Pedersen, K. B. Jakobsen, and M. Vaa, J. Lightwave Technol. **14**, 833 (1996).
5. K. Zoiros, T. Stathopoulos, K. Vlachos, *et al.*, Opt. Commun. **180**, 301 (2000).
6. I. Ozdur, M. Akbulut, N. Hoghooghi, *et al.*, IEEE Photonics Technol. Lett. **22**, 431 (2010).
7. A. Oran, S. Ozharar, G. Can, *et al.*, Opt. Express **26**, 376 (2018).
8. S. Min, Y. Zhao, and S. Fleming, Opt. Express **17**, 6187 (2009).
9. J. H. Kim, Y. M. Jhon, Y. T. Byun, *et al.*, IEEE Photonics Technol. Lett. **14**, 1436 (2002).
10. J. McGeehan, S. Kumar, D. Gurkan, *et al.*, J. Lightwave Technol. **21**, 2746 (2003).
11. K. Vlachos, C. Bintjas, N. Pleros, *et al.*, IEEE J. Sel. Top. Quantum Electron. **10**, 147 (2004).
12. S. J. Park, G. H. Kim, H. D. Lee, *et al.*, Appl. Sci. **9**, 4029 (2019).
13. K. Zoiros, M. Moyssidis, and T. Houbavlis, Optik **115**, 553 (2004).
14. M. Singh, A. K. Sharma, and R. Kaler, Optik **119**, 359 (2008).
15. G. Agrawal and N. Olsson, IEEE J. Quantum Electron. **25**, 2297 (1989).